ROYAL SOCIETY OF CHEMISTRY

PAPER

Check for updates

A study of complexation and biological fate of polyethyleneimine-siRNA polyplexes *in vitro* and *in vivo* by fluorescence correlation spectroscopy and positron emission tomography imaging†

Tanja Ludtke,[a] Cristina Simó, [ID] [a,b] Santiago Gimenez Reyes,[a,c] Marta Martinez Moro,[a] Cristian Salvador,[d] Hernan Ritacco, [ID] [c] Patrizia Andreozzi,[e] Jordi Llop [ID] *[b] and Sergio E. Moya [ID] *[a]

A deeper knowledge on the formation and biological fate of polymer based gene vectors is needed for their translation into therapy. Here, polyplexes of polyethyleneimine (PEI) and silencing RNA (siRNA) are formed with theoretical N/P ratios of 2, 4 and 12. Fluorescence correlation spectroscopy (FCS) is used to study the formation of polyplexes from fluorescently labelled PEI and siRNA. FCS proves the presence of free PEI. From the analysis of the autocorrelation functions it was possible to determine the actual stoichiometry of polyplexes. FCS and fluorescence cross correlation spectroscopy (FCCS) are used to follow the fate of the polyplexes intracellularly. Polyplexes disassemble after 1 day inside cells. Positron emission tomography (PET) studies are conducted with radiolabelled polyplexes prepared with siRNA or PEI labelled with 2,3,5,6-tetrafluorophenyl 6-[^{18}F]-fluoronicotinate ([^{18}F]F-PyTFP). PET studies in healthy mice show that [^{18}F]siRNA/PEI and siRNA/[^{18}F]PEI polyplexes show similar biodistribution patterns with limited circulation in the bloodstream and accumulation in the liver. Higher activity for [^{18}F]PEI in the kidney and bladder suggests the presence of free PEI.

Introduction

The latest developments in gene therapy allow for the treatment of practically any disease. However, translation of gene therapies to the clinic has been limited up to now, to a large extent because of the lack of appropriate vectors to protect the nucleic acids and facilitate their transport into cells.[1,2]

Exogeneous nucleic acids are easily degraded by nuclease enzymes, and being negatively charged, they are not easily taken up by cells. There are two main groups of vectors for nucleic acids in gene therapy: viral vectors,[3] which profit from the natural capacity of the virus for transfection, and non-viral vectors, usually positively charged polyelectrolytes or lipids.[4–9] In the latter, positive charges are used for complexation with the negatively charged nucleic acids, thus protecting them from enzymatic degradation and facilitating their translocation inside cells. Lipid-based vectors have been boosted by recent developments in SARS covid vaccines.[10,11] However, polymer-based vectors have several interesting advantages for gene delivery as they display multiple charges that can lead to a more effective osmotic swelling and triggering of polyplex translocation into the cytoplasm.[12–14] Polymer-based vectors also offer a huge range of possible modifications, such as peptide or antibody functionalization for targeted delivery.[15,16] Polyethyleneimine (PEI) is a polymer widely used in gene therapy. PEI is a polycation displaying primary, secondary, and tertiary amines and can be linear or branched. Branched PEI has been extensively used for gene therapy as it has a relatively low toxicity while providing many positive charges available for complexation with nucleic acids.[17–20] Positive charges in PEI play a fundamental role in polyplex translocation and endosomal scape.[21] Complexation of nucleic acids to PEI is performed by mixing polymer and nucleic acid solutions taking into account the balance of positive charges coming

[a]Soft Matter Nanotechnology, Center for Cooperative Research in Biomaterials (CIC biomaGUNE), Basque Research and Technology Alliance (BRTA), Paseo de Miramon 194, 20014 Donostia-San Sebastián, Spain. E-mail: smoya@cicbiomagune.es
[b]Radiochemistry and Nuclear Imaging laboratory, Center for Cooperative Research in Biomaterials (CIC biomaGUNE), Basque Research and Technology Alliance (BRTA), Paseo de Miramon 194, 20014 Donostia-San Sebastián, Spain.
E-mail: jllop@cicbiomagune.es
[c]Instituto de Fisica del Sur (IFISUR-CONICET), Av. Alem, Bahia Blanca, Argentina
[d]CIDETEC, Basque Research and Technology Alliance (BRTA), Parque Científico y Tecnológico de Gipuzkoa, Miramon Pasealekua, 196, Donostia-San Sebastián 20014, Spain
[e]Department of Chemistry 'Ugo Schiff', University of Florence, Via della Lastruccia 3, 50019 Sesto Fiorentino, FI, Italy
†Electronic supplementary information (ESI) available. See DOI: https://doi.org/10.1039/d3nr04026g

from the amines of PEI and negative charges coming from the phosphate groups of the nucleic acids. This balance is expressed by the N/P ratio,[22,23] which is calculated considering all protonable amines from the polymers (N) and all phosphate groups in the nucleic acids (P). However, not all charges are always used for complexation. Complexation depends on the accessibility of the charges, which can vary depending on the type of nucleic acid: silencing RNA (siRNA), messenger RNA (mRNA), plasmids, etc.[24] siRNA, although double stranded, is a short molecule and most of the charges are accessible for complexation, but this is not necessarily the case for plasmids. In addition, the complexation will be affected if the polymers are linear or branched, as not all amines may be available for complexation with the nucleic acids in a branched configuration.[25] Therefore, the N/P ratios calculated may not reflect the actual stoichiometry of the polyplexes. The actual composition of the polyplexes in terms of nucleic acids and polymers is not easy to determine, as it is difficult to separate unbound polymer or siRNA from the polyplex solution.

Despite its practical relevance, there are limited studies based on the biological fate of PEI polyplexes. Co-localization studies of fluorescent nucleic acids and PEI inside cells have been conducted by confocal laser scanning microscopy (CLSM), which allows one to follow translocation of the nucleic acids inside the cells.[26] Nevertheless, there are even fewer works addressing the biological fate of siRNA complexed with PEI and the stability of the resulting polyplexes *in vivo*. This lack of knowledge is to a large extent due to the overall difficulties in tracing exogenous nucleic acids inside *in vivo* models.

In this work, we aimed to contribute knowledge on the formation of branched PEI/siRNA polyplexes and their biological fate by performing a combined study involving fluorescence correlation spectroscopy (FCS),[27] fluorescence cross correlation spectroscopy (FCCS),[28] and positron emission tomography (PET).[29] By FCS/FCCS using both labelled PEI and siRNA we analysed the organization of polyplexes and determined the actual stoichiometry of the complexes as well as the percentage of unbound polymer in conditions of excess polymer for polyplex formation. FCCS was applied to trace the fate of polyplexes inside A549 cells by measuring changes in the cross correlation of the two components. Cross correlation functions are not affected by free polymer that could be present in bulk prior to cell uptake, thus providing unequivocal information on the fate of the complexes. Using FCCS we determined the time taken for the complexes to disassemble. Finally, we conducted *in vivo* studies of the polyplexes by PET imaging using either radiolabelled PEI or siRNA[30] to trace the biological fate of each component of the polyplexes, and to study the stability of the polyplexes following intravenous administration in rodents. PET studies confirmed the presence of non-complexed PEI *in vivo*.

Materials and methods

Chemistry

Reagents. PEI (M_w = 25 kDa) was purchased from SIGMA. All FCS/FCCS experiments were performed with branched PEI (M_w

= 25 kDa) labelled with green rhodamine (provided by Surflay Nanotec GmbH) as well as commercially available Cy5-labelled siRNA (13 kDa, MISSION, Sigma-Aldrich Co. LLC). The emission maximum of green rhodamine is at 527 nm and of Cy5 at 666 nm.

Penicillin and streptomycin were purchased from Sigma Aldrich. Rhodamine 123, DPBS (Gibco) and FBS were purchased from Thermo Fisher Scientific. Human cell line A549 lung adenocarcinoma and Eagle's Minimum Essential Medium (EMEM) were obtained from the American Type Culture Collection (ATCC), USA. Uranyl acetate was purchased from. Electron Microscopy Sciences (EMS), USA. For *in vivo* studies, negative control siRNA-duplex was purchased from BioSpring Company (Frankfurt, Germany) with an antisense strand 5′ amino C6 linker modification. UPLC-grade RNAse-free water was purchased from Sigma Aldrich.

Polyplex formation:. A fixed amount of PEI was diluted in RNAse free water to a concentration of 1 μM with a final volume of 50 μL. Separately, an adjusted concentration of siRNA to yield N/P ratios of 2, 4 and 12 was diluted with RNAse free water to reach a final volume of 50 μL. Both solutions were combined, mixed, and left for 30 minutes at room temperature for particle assembly to take place. N/P ratio was calculated only considering protonable amines from PEI.

Characterisation and *in vitro* studies

Transmission electron microscopy. Carbon-coated copper grids (Ted Pella, Inc.) were hydrophilized, and 1.5 μL of the sample was applied and left to incubate on the grid for 3 minutes. Excess solution was removed with filter paper and 1.5 μL of 1.5% uranyl acetate solution for positive staining was added to the grid and left for 3 minutes, followed by two washing steps. Imaging was conducted with a LaB$_6$-TEM of type JEOL JEM-1400PLUS (40 kV–120 kV, HC pole piece) equipped with a GATAN US1000 CCD camera (2k × 2k). TEM images were analysed using the software ImageJ.

Fluorescence cross correlation spectroscopy. FCCS measurements were recorded with a Zeiss LSM 880 confocal microscope and analysed with Zen black software. A HeNe-laser was used for excitation at 633 nm and an Ar-laser for excitation at 488 nm. Emission was recorded using GaAsP (510–560 nm) and PMT (650–715 nm) detectors. Measurements were conducted with a Zeiss C-Apochromat 40×, numerical aperture 1.2 water immersion objective. 100 μL of the particle dispersion was filled up to 200 μL final sample volume and transferred to a chambered polymer coverslip (ibidi) for FCCS measurement. Prior to sample measurement, the confocal volume was calibrated with a 30 nM solution of Rhodamine 123 in UHPLC-grade water using a diffusion coefficient[31] of 440.00 μm² s⁻¹ for the analysis of PEI and the green rhodamine. Confocal volume was determined with ATTO 633 with a diffusion coefficient of 340.00 μm² s⁻¹ for the analysis of siRNA. One measurement consisted of 20 runs of 20 seconds. The data fitting was done with QuickFit software[3 32] using the global fit of 1, 2 and 3-components and 3D normal diffusion model. The resulting diffusion coefficients were used to calcu-

late the hydrodynamic diameter D_H with the Stokes–Einstein equation.

Cell culture. Cells (lung adenocarcinoma A549) were cultured at 37 °C in an atmosphere with 5% CO_2 in RPMI 1640 medium, which contains 10% FBS and 1% *P/S* (100 units per mL penicillin, 100 mg mL^{-1} streptomycin).

Intracellular FCCS. A549 lung adenocarcinoma cells were prepared at least 24 h before FCCS measurements by seeding 4 × 10^{-4} cells in an ibidi 8-well chambered polymer coverslip with 250 μL MEM containing 10% FBS and 1% *P/S*. The medium was removed, and the cells washed with Dulbecco's phosphate buffered saline (DPBS) before adding PEI/siRNA polyplexes with ratios N/P = 2 and 4 and letting them incubate for 1 h. Cells were washed three times and kept in DPBS for the measurement. After the initial FCCS measurement the cells were embedded in fresh medium and stored in a humidified chamber at 37 °C at 5% CO_2 overnight. A second set of measurements was performed after 24 h. Triplicate measurements were conducted at different positions inside the cells.

Radiochemistry

Synthesis of [¹⁸F]F-PyTFP. Preparation of 2,3,5,6-tetrafluorophenyl 6-[¹⁸F]-fluoronicotinate ([¹⁸F]F-PyTFP) was performed in Neptis® xSeed™ module (Optimized Radiochemical Applications, ORA) following a previously described method.[33]

Radiolabelling of siRNA with [¹⁸F]F-PyTFP. The ¹⁸F-labelled siRNA was prepared by incubating siRNA containing an amino group-modification with [¹⁸F]F-PyTFP. In brief, 6 μL of siRNA in 50 mM borate buffer pH 8.5 (80.5 μg μL^{-1}) was incubated with 3 μL of [¹⁸F]F-PyTFP in acetonitrile (ACN; 92,5 ± 18.5 MBq) at room temperature for 20 min. After incubation, the reaction mixture was purified by size exclusion chromatography using Illustra™ Nap™-5 Sephadex™ columns G-25 DNA grade (GE Healthcare, USA), preconditioned with physiologic saline solution (for siRNA to be directly injected into animals) or water (for siRNA complexed with PEI, see below). The fractions containing pure labelled siRNA were collected and measured in a dose calibrator. The radiochemical purity was measured by high performance liquid chromatography (HPLC) using an Agilent 1200 series system equipped with a quaternary pump, multiple wavelength detector (wavelength set at 254 nm) and radiometric detector (Gabi, Raytest). A C18 Mediterranean column (4.6 × 150 mm, 5 μm; Teknokroma, Spain) was used as the stationary phase, and 0.1 M triethylammonium acetate (TEAA) buffer pH 7.4 and ACN as the mobile phase (Gradient: 1 min 5% ACN, 5 min 10% ACN, 14 min 30% ACN, 20–22 min 50% ACN, 25 min 5% ACN) at a flow rate of 1.0 mL min^{-1} (retention time = 10–11 min). Radiochemical stability studies of the labelled SiRNA were carried out up to 6 h after preparation using the same analytical technique and conditions.

Radiolabelling of PEI with [¹⁸F]F-PyTFP. PEI was radiolabelled by incubation of the polymer with [¹⁸F]F-PyTFP. In brief, 200 μL of PEI (1 mg mL^{-1}) in ultrapure water was mixed with 5 μL of [¹⁸F]F-PyTFP (111 MBq), and incubated at room temperature for 5 min. The resulting solution was used for polyplex formation without further purification. Quality control of radiolabelled PEI was carried out by radio-thin layer chromatography (radio-TLC) reader (MiniGITA, Raytest) using i-TLC chromatographic paper (Agilent Technologies, CA, USA) as the stationary phase, and dichloromethane : methanol (2 : 1) as the mobile phase. R_f values for PEI and [¹⁸F]F-PyTFP were 0–0.1 and 0.5–0.6 cm, respectively. Radiochemical stability studies of the labelled polymer were carried out up to 6 h after preparation using the same analytical technique and conditions.

Polyplex formation with ¹⁸F-siRNA or ¹⁸F-PEI. Polyplex formation was performed as described above but using the radioactive equivalent.

In vivo studies

Animals. Biodistribution studies were performed in female BALB/c mice (8 weeks, Janvier Labs, N = 9). Animals were maintained and handled in accordance with the Guidelines for Accommodation and Care of Animals (European Convention for the Protection of Vertebrate Animals Used for Experimental and Other Scientific Purposes) and internal guidelines. All experimental procedures were approved by the internal ethical committee and the local authorities before conducting experimental work (authorization code: PRO-AE-SS-207).

Biodistribution studies. Animals were anesthetized by inhalation of 3% isoflurane in pure O_2 and maintained by 1.5–2% isoflurane in 100% O_2. With the animal under anaesthesia, *ca.* 110 μL of ¹⁸F-PEI/siRNA or PEI/¹⁸F-siRNA polyplexes were administered intravenously (*via* one of the lateral tail veins) using saline as a vehicle. Immediately after administration, 30-minute dynamic whole-body PET scans were acquired using a MOLECUBES β-CUBE scanner (MOLECUBES, Gent, Belgium). 10 min static PET scans were performed 4 hours after administration. After each PET scan, whole body high resolution computerized tomography (CT) acquisitions were performed using a MOLECUBES X-CUBE scanner (MOLECUBES, Gent, Belgium) to provide anatomical information of each animal as well as the attenuation map for the later image reconstruction.

PET images were reconstructed using the 3D OSEM reconstruction algorithm and applying random, scatter and attenuation corrections. PET-CT images of the same animal were co-registered and analysed using the PMOD image processing tool (PMOD Technologies LLC, Switzerland; version 3.4). Volumes of interest (VOIs) were manually delineated in organs clearly visualized on CT images (brain, heart, lungs, liver, kidneys, and bladder). VOIs were also drawn in the spleen and the stomach, to obtain estimative values of concentration of radioactivity. Activity values (decay-corrected) were obtained as KBq cm^{-3} and corrected by applying a calibration factor obtained from previous scans on a phantom (micro-deluxe, Data spectrum Corp.) under the same experimental conditions (isotope, reconstruction, algorithm, and energy window). Time-activity curves were expressed as percentage of injected dose per cm^3 of tissue (% ID cm^{-3}) over time (min).

Results and discussion

PEI and siRNA solutions were mixed for three selected molar ratios of protonable amines from the branched PEI and phosphate groups from siRNA, corresponding to N/P = 2, 4 and 12 (Scheme 1).

Polyplexes were formed in RNAse free water, drop casted onto TEM grids, and positively stained with uranyl acetate. TEM images and size distribution analyses show a trend of aggregation of the nanoparticles, which is more pronounced the higher the N/P ratio (Fig. 1). TEM images for N/P = 2 and 4 suggest the presence of free polymer on the grids, which is visualized as stains with lower contrast than the particles.

An increase in particle size was observed when increasing the N/P ratio. Polyplexes have an average radius of 22.8 ± 5.5 nm at N/P = 2, 26.8 ± 8.1 nm at N/P = 4, and 41.2 ± 13.6 nm at N/P = 12.

The size of the polyplexes was further characterized by their diffusion, using FCS and FCCS and labelled PEI and siRNA. The diffusion coefficients of single PEI (D_{PEI} = 50 μm² s⁻¹) and siRNA (D_{siRNA} = 55 μm² s⁻¹) were estimated prior to complexation. These values were used for fitting the resulting cross correlation (CC) of the polyplexes with N/P = 2, 4 and 12. The autocorrelation functions (ACF_G-PEI and ACF_R-siRNA), are shown in Fig. 2 and their respective cross-correlation in Fig. S1.† Table S1† shows the corresponding values for diffusion coefficient and hydrodynamic diameter.

A first interesting conclusion from the autocorrelation curves is that the number of diffusing species is not the same for siRNA and PEI, which means that not all molecules are forming the polyplexes. Since PEI is always in excess in all the polyplex preparations, and the amplitude of the autocorrelation curves of siRNA is much larger than that of PEI, and the autocorrelation is inversely proportional to the number of species; it can be deduced that not all PEI is bound to the siRNA and a fraction of PEI remains free, diffusing in solution. Since all siRNA must complex with PEI in an excess of PEI, it can be assumed that the amplitude of the autocorrelation curve of siRNA, which is inversely proportional to the number of species with siRNA, corresponds to the actual number of
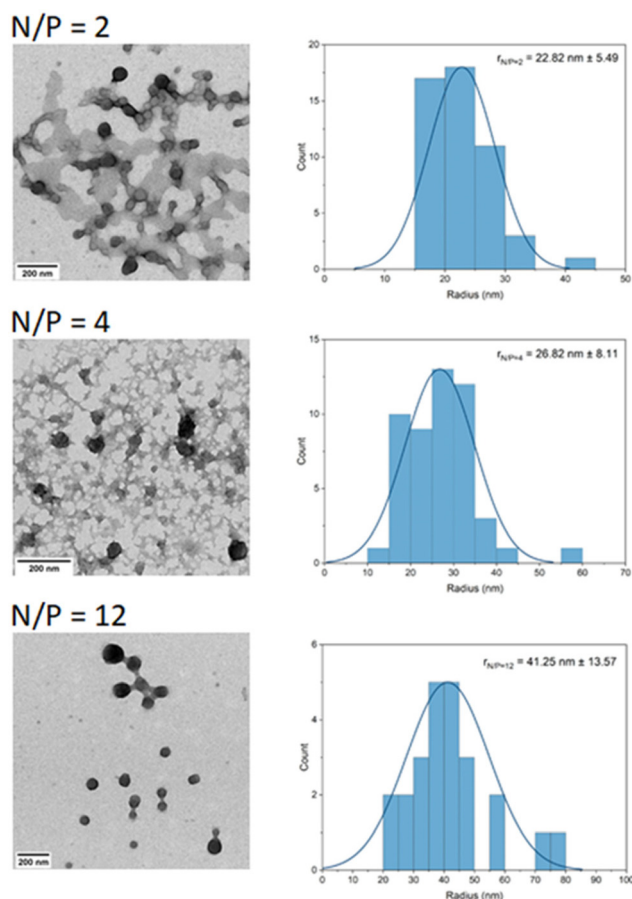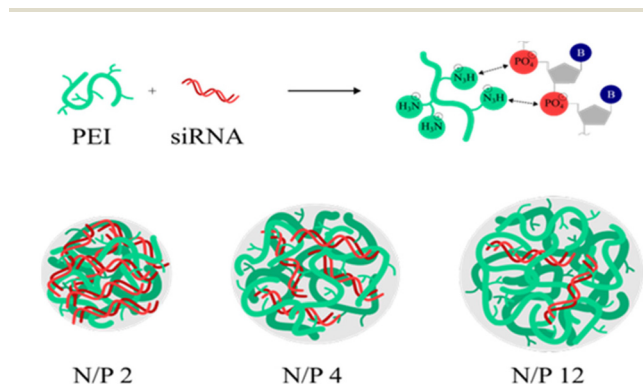

Fig. 1 TEM images and size distribution histograms of PEI/siRNA polyplexes with N/P ratios = 2, 4 and 12, and the resulting radii after measurement of 50 counts for N/P = 2 and 4 and 24 counts for N/P = 12.

polyplexes formed. This hypothesis was confirmed by the fitting of ACF_R-siRNA where the obtained fraction of free siRNA was equal to zero. The number of PEI diffusing species includes the polyplexes and free PEI. From the fitting of the autocorrelation curve of green rhodamine labelled PEI, and assuming the same diffusion coefficient for siRNA and complexed PEI (see explanation in ESI†), the fraction of free PEI could be obtained. For theoretical N/P values of 2, 4 and 12, FCS analysis revealed effective N/P values of 1.5 ± 0.1, 3.1 ± 0.2 and 7.1 ± 0.2, respectively. Since the number of siRNA molecules is known, and the number of PEI molecules used for the formation of the complexes can be estimated, the number of siRNA and PEI molecules per polyplex can be calculated by dividing these numbers by the number of polyplexes. This calculation results in approximately 15 ± 2 siRNA and 5.2 ± 0.7 PEI molecules for N/P = 2; 15 ± 2 siRNA and 11 ± 1 PEI molecules for N/P = 4; and 3.8 ± 0.4 siRNA and 6.2 ± 0.8 PEI molecules for N/P = 12 (see ESI† for further details).

Following characterization of the polyplexes by FCS, the fate of polyplexes with N/P = 2 and N/P = 4 was further investigated by FCCS following internalization in A549 lung adenocarcinoma cells. Measurements were carried out at 1 h and
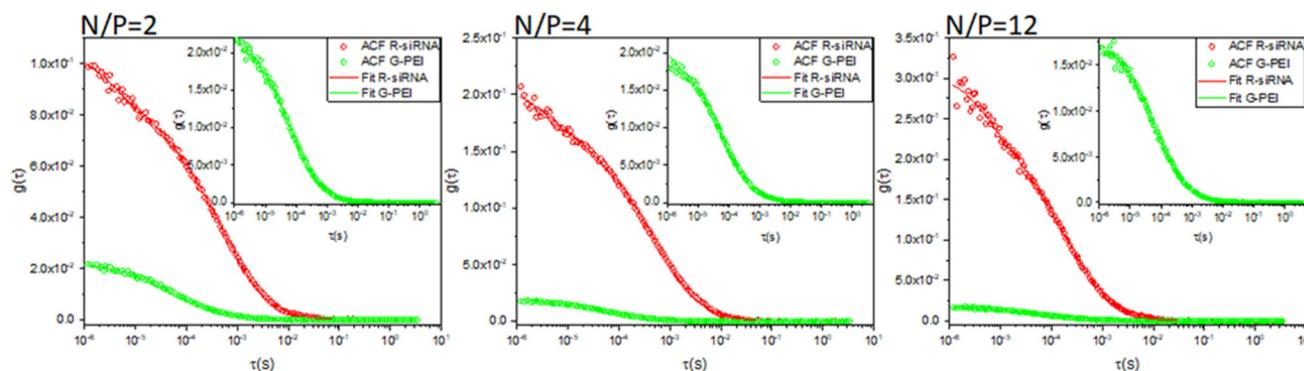

Scheme 1 Formation of polyplexes based on the complexation of siRNA and PEI at the three selected N/P ratios.

Fig. 2 Autocorrelation functions of siRNA (ACF_R-siRNA) in red and PEI (ACF_G-PEI) in green with their fittings (solid lines) for the different N/P ratios from *in vitro* experiments.

24 h after transfection (see Fig. 3 for N/P = 4, Fig. S2 and S3† for N/P = 2; see Table S2† for summarised data).

The locations in the cell where FCCS measurements were conducted are shown by crosshairs in confocal images (Fig. 3, top left). Immobile fluorescent species emit high intensity fluorescence, requiring a bleaching of the sample for 180 seconds prior to the FCCS data acquisition. The decrease in fluorescence signal (top graphs in Fig. 3A and B), which confirm bleaching events, is associated with a high amount of immobile polyplexes that are attached to the cell structure and not able to diffuse through the cytoplasm.[7] After bleaching, the subsequent FCS measurements provide information on the diffusion behaviour of the mobile polyplexes and the association of the differently labelled components, which is shown by the autocorrelation functions, ACF_G-PEI and ACF_R-siRNA, and the magnified representation of the CC in Fig. 3A and B (bottom). The low diffusion coefficients at $t = 1$ h ($D_{NP2\ d1} = 0.27\ \mu m^2\ s^{-1} \pm 0.07$; $D_{NP4\ d1} = 0.33\ \mu m^2\ s^{-1} \pm 0.19$) and high hydrodynamic diameters (D_H) for the polyplexes (see Table S2†) indicate successful uptake of the self-assembled nanoparticles inside the cell after 1 h of incubation. The progressive increase in diffusion coefficients in the cell environment, which is more abrupt for N/P = 4 than for N/P = 2 ($D_{NP2\ d2} = 0.46\ \mu m^2\ s^{-1} \pm 0.25$ and $D_{NP4\ d1} = 1.11\ \mu m^2\ s^{-1} \pm 0.60$ at $t = 24$ h) suggest a disassembly of the nanoparticles after cell uptake and therefore a release of siRNA.

Moreover, comparing the amplitude of cross correlation (ACC) of both N/P ratios on day 1 and day 2 supports the conclusion that the particles disassemble, thus leading to the liberation of siRNA. The average ACC of the particles with N/P = 2 decreases from 2.03×10^{-4} to 1.43×10^{-4} meaning that the co-localization of PEI and siRNA decreases. In the case of N/P = 4 the average ACC on day 1 is 4.18×10^{-4}, which decreases to 3.93×10^{-5} after 24 h (Fig. 3B).

To increase our understanding of the biological fate of PEI/siRNA polyplexes, we conducted *in vivo* studies using PET imaging in combination with CT. PET is a minimally invasive, ultra-sensitive nuclear imaging technique that enables distribution studies of positron emitter-labelled molecules after

administration in living organisms. With this aim, fluorine-18 ([18F]), a widely used radionuclide in the clinical setting, was selected as the positron emitter to radiolabel siRNA or PEI. For tracing siRNA, a modified siRNA with an additional amino group was purchased to be functionalized with a pre-labelled prosthetic group ([18F]F-PyTFP). For PEI, we used the same labelling strategy. Despite other labelling strategies using longer-lived radionuclides have been reported for the radiolabelling of PEI,[34] our approach based on the preparation of the prosthetic group [18F]F-PyTFP was considered to be more convenient because (i) the preparation of the labelling agent ([18F]F-PyTFP) is well established in our laboratory; (ii) the strategy can be used for both siRNA and PEI; and (iii) [18F] is widely available and has favourable emission properties (100% positron emission decay and short positron range).

In the case of siRNA, radiochemical yields of 25 ± 5% (with respect to [18F]F-PyTFP, decay-corrected) were achieved by 20 min incubation at room temperature, and the radiochemical purity was ≥95% as determined by radio-HPLC (see Fig. S4† for representative chromatograms before and after purification). For radiolabelling of PEI, the procedure was the same as used for siRNA, but taking advantage of the multiple amino groups present on the polymer chain to react with [18F]F-PyTFP. In this case, the radiochemical yield and radiochemical purity were ≥95% (see Fig. S5† for representative chromatogram). [18F]-PEI proved stable up to 6 h after preparation, with radiochemical purity values above 95% over the whole period (Fig. S6†). However, SiRNA showed good stability only over the first 2 hours after preparation. At $t = 4$ hours, the presence of a radioactive broad peak in the HPLC profile (Fig. S7†) suggests the formation of undesired labelled species. To prevent interference with our studies, administration of SiRNA (or PEI/[18F]-siRNA) was always carried out within this time window (0–2 h after preparation).

After radiolabelling of the individual components, PEI/siRNA polyplexes were prepared with a N/P of 4. Biodistribution studies were conducted after intravenous administration of radiolabelled polyplexes (Fig. 4 and S8†). Visual inspection of the PET images and image quantification
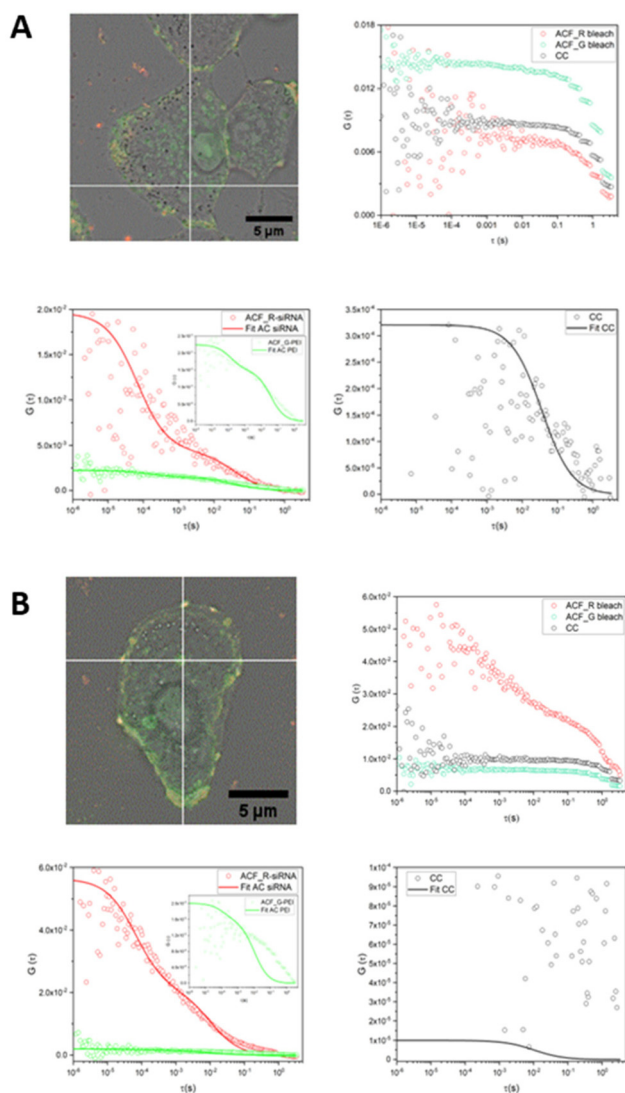
Fig. 3 FCCS measurements of PEI and siRNA at $t = 1$ h (A) and $t = 24$ h (B) after transfection of the cells. In the images, crosshairs show the position of measurement. Due to immobile PEI and siRNA, a bleaching was performed before FCS measurements, leading to a decrease in the signal intensity (top right). The resulting autocorrelation functions (red and green curves; bottom left), and the cross-correlation function (black; bottom right) are shown. After 24 h the CC decreased compared with the measurement taken 1 h after the transfection.

revealed a similar biodistribution profile, with slight differences, for both polyplexes independent of tracking ^{18}F-PEI or ^{18}F-siRNA. Biodistribution of PEI/^{18}F-siRNA complex showed a low radioactivity accumulation in heart (surrogate of the concentration of radioactivity in blood), with its maximal value in the first 5 minutes (*ca.* 20% ID cm^{-3}) and decreasing progressively afterwards. This result suggests a rapid clearance from the blood and immediate accumulation in the other organs. Similar profiles were obtained in the lungs and kidneys, with maximum accumulation of radioactivity in the first-time frame (0–5 min). Activity in brain and stomach was very low. The maximum accumulation of radioactivity was obtained in the

liver (Fig. 4) and in the spleen (Fig. S8†), where was practically constant during the whole dynamic imaging study, suggesting a possible aggregation of the nanoparticles in the blood stream that would result in their clearance by the MRS system and accumulation in the liver. Noteworthy, spleen values need to be considered as estimative due to the difficulties associated to VOI delineation. This biodistribution profile is typical of nanoparticles with larger sizes than those obtained by TEM in Fig. 1. However, polyplexes are positively charged, so they can interact with biomolecules and aggregate this way. The presence of radioactivity in urine suggests progressive release of the ^{18}F-siRNA, probably due to disassembly of the polyplexes by the negatively charged glycans in kidney.[35,36] Indeed, control experiments consisting of intravenous administration of free ^{18}F-siRNA showed a rapid accumulation of radioactivity in the kidneys and the bladder, confirming a rapid clearance of the siRNA from the body *via* urinary excretion (Fig. S9†).

When ^{18}F-PEI was traced in the polyplex instead of siRNA, a slightly different biodistribution pattern was observed. Similar values of radioactivity were obtained in the liver, which remained constant until the end of the imaging study. However, higher values of accumulation were observed in the kidneys and bladder with respect to the PEI/^{18}F-siRNA complex. The presence of free branched ^{18}F-PEI, which has a size of 8.7 nm in diameter as calculated from FCS measurements and could be easily filtrated by the kidneys and eliminated *via* urine (below 10 nm), may explain the presence of radioactivity in urine. This hypothesis is in agreement with FCS data (Fig. 2). In fact, radioactivity was also found in the bladder for PEI/^{18}F-siRNA complex, suggesting a possible cleavage of the polyplex *in vivo*. The concentration in the kidneys and bladder shortly after intravenous administration was higher for ^{18}F-PEI/siRNA than for PEI/^{18}F-siRNA, which also suggests that free ^{18}F-PEI might have been injected with the polyplexes.

We have determined by FCS/FCCS that the stoichiometry of the polyplexes of PEI and siRNA is not necessarily as calculated when mixing PEI and siRNA taking into account the number of positive and negative charges (N/P ratio of protonable amines of PEI to phosphate groups of siRNA). Assuming that all siRNA forms the complex in an excess of PEI, the number of polyplexes equals the number of diffusing species containing siRNA, and this number can be obtained from the amplitude of the autocorrelation curves for siRNA. The smaller amplitude of the autocorrelation curve for the PEI with respect to siRNA confirms that the number of species with PEI is much larger, and consequently there is non-complexed PEI in solution. Once the percentage of free PEI in solution is known, FCCS becomes a very powerful tool to investigate the fate of the polyplexes in cells, as time-resolved changes in the degree of co-localization of siRNA and PEI can be determined from the amplitude of the CC and from changes in the function of auto correlation of the individual components. In this way, the presence of free PEI in solution before cell uptake does not alter the conclusions, even if free labelled PEI is internalized by the cells influencing the initial cross correlation measure-
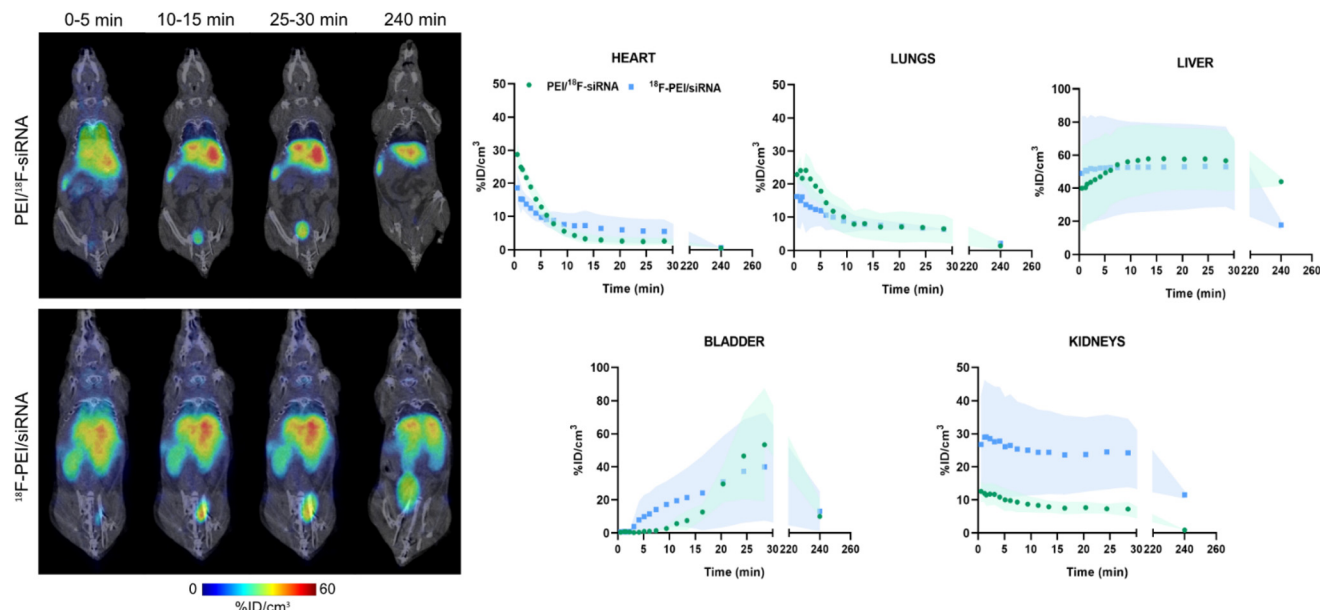
Fig. 4 Left, representative PET images (coronal views, maximum intensity projection) obtained after intravenous administration of ^{18}F-PEI/siRNA and PEI/^{18}F-siRNA complexes at different time points. Images were co-registered with representative CT slices. Right, concentration of radioactivity in different organs after administration of ^{18}F-PEI/siRNA and PEI/^{18}F-siRNA complexes at different time points, determined by PET imaging quantification. Results are expressed as % of injected dose per cm³ of tissue (%ID/cm³; average ± standard deviation, n = 3 per type of polyplex).

ments, as variations in cross correlation are indeed the indicator of the rupture of the polyplex. FCCS provides a means to measure how the concentration of double labelled species of PEI and siRNA is changing, which is not affected by the presence of free PEI. FCC shows a decrease in the auto correlation function with time as the complex disassembly, and cross-correlation values are the lowest after 24 h.

In vivo, by comparing the biodistribution of polyplexes synthesized using either radiolabelled PEI or siRNA and the biodistribution of free radiolabelled siRNA, we can conclude that the complexation of siRNA with PEI results in clear changes in the fate of the siRNA. Polyplex circulation is short as the concentration of radioactivity in the heart decreases rapidly after administration. The presence of radioactivity in the kidneys and the bladder after administration of ^{18}F-PEI/siRNA could be due to the presence of small polyplexes, with sizes that allow for their filtering through kidneys and subsequent elimination *via* urine. When we look at the biodistribution of the polyplexes labelled through PEI we observe similar biodistribution patterns in liver, lungs, and heart as for polyplexes labelled through the siRNA. In kidneys and bladder, activity is higher for the labelled PEI, even from the initial measurements. This result suggests that there is free PEI circulating. Branched PEI can be filtered through the kidneys and then eliminated through the bladder. *In vivo* experiments show differences in the biodistribution of siRNA and PEI, suggesting that the solution of the polyplexes is a mixture of polyplexes and free PEI, confirming conclusions from FCS in bulk. We chose a N/P of 4 for these experiments as it is the intermediate value among the 3 N/P ratios used for FCS and because there are not so

large differences in the size of the polyplexes, ranging between 22 nm (N/P 2) and 41 nm (N/P 12). Since sizes are similar, we can expect a similar biodistribution for the three polyplexes. However, we can not rule out that *in vivo* stability would be the same for all the N/P ratio. Further experiments will focus on this issue.

Conclusions

We studied PEI/siRNA polyplex formation and biological fate by FCS/FCCS and PET imaging, which provide unique information on these processes that cannot be easily obtained by other means. The study of the formation of the polyplexes of siRNA and PEI by FCS for different N/P ratios reveals that there is always some free PEI, not complexed with the siRNA. PET imaging suggests as well that free PEI is injected into the animals together with the polyplexes. PET imaging shows a rapid accumulation of the polyplexes in the liver and limited circulation within 20 min. FCCS in cells reveals that the complexes largely disassemble within one day after uptake.

Author contributions

We strongly encourage authors to include author contributions and recommend using CRediT for standardised contribution descriptions. Please refer to our general author guidelines for more information about authorship.

Conflicts of interest

There are no conflicts to declare.

Acknowledgements

References

1 S. Mirón-Barroso, E. B. Domènech and S. Trigueros, Nanotechnology-Based Strategies to Overcome Current Barriers in Gene Delivery, *Int. J. Mol. Sci.*, 2021, **22**(16), 8537.

2 R. Mohammadinejad, A. Dehshahri, V. S. Madamsetty, M. Zahmatkeshan, S. Tavakol, P. Makvandi, D. Khorsandi, A. Pardakhty, M. Ashrafizadeh, E. Ghasemipour Afshar and A. Zarrabi, In Vivo Gene Delivery Mediated by Non-Viral Vectors for Cancer Therapy, *J. Controlled Release*, 2020, **325**, 249–275.

3 J. T. Bulcha, Y. Wang, H. Ma, P. W. L. Tai and G. Gao, Viral Vector Platforms within the Gene Therapy Landscape, *Signal Transduction Targeted Ther.*, 2021, **6**(1), 53.

4 M. L. Forrest, J. T. Koerber and D. W. Pack, A Degradable Polyethylenimine Derivative with Low Toxicity for Highly Efficient Gene Delivery, *Bioconjugate Chem.*, 2003, **14**(5), 934–940.

5 E. Baghdan, S. R. Pinnapireddy, B. Strehlow, K. H. Engelhardt, J. Schäfer and U. Bakowsky, Lipid Coated Chitosan-DNA Nanoparticles for Enhanced Gene Delivery, *Int. J. Pharm.*, 2018, **535**(1–2), 473–479.

6 X. Yuan, B. Qin, H. Yin, Y. Shi, M. Jiang, L. Luo, Z. Luo, J. Zhang, X. Li, C. Zhu, *et al.* Virus-like Nonvirus Cationic Liposome for Efficient Gene Delivery via Endoplasmic Reticulum Pathway, *ACS Cent. Sci.*, 2020, **6**(2), 174–188.

7 D. Di Silvio, M. Martínez-Moro, C. Salvador, M. de los Angeles Ramirez, P. R. Caceres-Velez, M. G. Ortore, D. Dupin, P. Andreozzi and S. E. Moya, Self-Assembly of Poly(Allylamine)/SiRNA Nanoparticles, Their Intracellular Fate and SiRNA Delivery, *J. Colloid Interface Sci.*, 2019, **557**, 757–766.

8 H. Yin, R. L. Kanasty, A. A. Eltoukhy, A. J. Vegas, J. R. Dorkin and D. G. Anderson, Non-Viral Vectors for Gene-Based Therapy, *Nat. Rev. Genet.*, 2014, **15**(8), 541–555.

9 L. Ke, P. Cai, Y. Wu and X. Chen, Polymeric Nonviral Gene Delivery Systems for Cancer Immunotherapy, *Adv. Ther.*, 2020, **3**(6), 1900213.

10 R. Tenchov, R. Bird, A. E. Curtze and Q. Zhou, Lipid Nanoparticles—From Liposomes to MRNA Vaccine Delivery, a Landscape of Research Diversity and Advancement, *ACS Nano*, 2021, **15**(11), 16982–17015.

11 A. Mehta, T. Michler and O. M. Merkel, SiRNA Therapeutics against Respiratory Viral Infections—What Have We Learned for Potential COVID–19 Therapies? Adv, *Healthcare Mater.*, 2021, **10**(7), 2001650.

12 I. A. Khalil, K. Kogure, H. Akita and H. Harashima, Uptake Pathways and Subsequent Intracellular Trafficking in Nonviral Gene Delivery, *Pharmacol. Rev.*, 2006, **58**(1), 32–45.

13 I. M. S. Degors, C. Wang, Z. U. Rehman and I. S. Zuhorn, Carriers Break Barriers in Drug Delivery: Endocytosis and Endosomal Escape of Gene Delivery Vectors, *Acc. Chem. Res.*, 2019, **52**(7), 1750–1760.

14 B. Xu, Y.-J. Zhu, C.-H. Wang, C. Qiu, J. Sun, Y. Yan, X. Chen, J.-C. Wang and Q. Zhang, Improved Cell Transfection of SiRNA by PH-Responsive Nanomicelles Self-Assembled with MPEG- b -PHis- b -PEI Copolymers, *ACS Appl. Mater. Interfaces*, 2018, **10**(26), 21847–21860.

15 C. Liu, Y. Xie, X. Li, X. Yao, X. Wang, M. Wang, Z. Li and F. Cao, Folic Acid/Peptides Modified PLGA–PEI–PEG Polymeric Vectors as Efficient Gene Delivery Vehicles: Synthesis, Characterization and Their Biological Performance, *Mol. Biotechnol.*, 2021, **63**(1), 63–79.

16 L. Liu, Y. Yan, D. Ni, S. Wu, Y. Chen, X. Chen, X. Xiong and G. Liu, TAT-Functionalized PEI-Grafting Rice Bran Polysaccharides for Safe and Efficient Gene Delivery, *Int. J. Biol. Macromol.*, 2020, **146**, 1076–1086.

17 O. Boussif, F. Lezoualc'h, M. A. Zanta, M. D. Mergny, D. Scherman, B. Demeneix and J. P. Behr, A Versatile Vector for Gene and Oligonucleotide Transfer into Cells in Culture and in Vivo: Polyethylenimine, *Proc. Natl. Acad. Sci.*, 1995, **92**(16), 7297–7301.

18 S. Mahajan and T. Tang, Polyethylenimine–DNA Nanoparticles under Endosomal Acidification and Implication to Gene Delivery, *Langmuir*, 2022, **38**(27), 8382–8397.

19 C. Gallops, J. Ziebarth and Y. Wang, in *A Polymer Physics Perspective on Why PEI Is an Effective Nonviral Gene Delivery Vector*, 2020, pp. 1–12.

20 C. Jiang, J. Chen, Z. Li, Z. Wang, W. Zhang and J. Liu, Recent Advances in the Development of Polyethylenimine-Based Gene Vectors for Safe and Efficient Gene Delivery, *Expert Opin. Drug Delivery*, 2019, **16**(4), 363–376.

21 E. Boonstra, H. Hatano, Y. Miyahara, S. Uchida, T. Goda and H. Cabral, A proton/macromolecule-sensing approach distinguishes changes in biological membrane permeability during polymer/lipid-based nucleic acid delivery, *J. Mater. Chem. B*, 2021, **9**, 4298–4302.

22 S. Mehrotra, I. Lee and C. Chan, Multilayer Mediated Forward and Patterned SiRNA Transfection Using Linear-PEI at Extended N/P Ratios, *Acta Biomater.*, 2009, **5**(5), 1474–1488.

23 A. C. Grayson, A. M. Doody and D. Putnam, Biophysical and Structural Characterization of Polyethylenimine-Mediated SiRNA Delivery in Vitro, *Pharm. Res.*, 2006, **23**(8), 1868–1876.

24 S. Mahajan and T. Tang, Polyethylenimine–DNA Ratio Strongly Affects Their Nanoparticle Formation: A Large-Scale Coarse-Grained Molecular Dynamics Study, *J. Phys. Chem. B*, 2019, **123**(45), 9629–9640.

25 L. Wightman, R. Kircheis, V. Rössler, S. Carotta, R. Ruzicka, M. Kursa and E. Wagner, Different Behavior of Branched and Linear Polyethylenimine for Gene Deliveryin Vitro Andin Vivo, *J. Gene Med.*, 2001, **3**(4), 362–372.

26 B. Urban-Klein, S. Werth, S. Abuharbeid, F. Czubayko and A. Aigner, RNAi-Mediated Gene-Targeting through Systemic Application of Polyethylenimine (PEI)-Complexed SiRNA in Vivo, *Gene Ther.*, 2005, **12**(5), 461–466.

27 M. Martinez-Moro, D. Di Silvio and S. E. Moya, Fluorescence Correlation Spectroscopy as a Tool for the Study of the Intracellular Dynamics and Biological Fate of Protein Corona, *Biophys. Chem.*, 2019, **253**, 106218.

28 P. Schwille, J. Bieschke and F. Oehlenschläger, Kinetic Investigations by Fluorescence Correlation Spectroscopy: The Analytical and Diagnostic Potential of Diffusion Studies, *Biophys. Chem.*, 1997, **66**(2–3), 211–228.

29 C. Pérez-Campaña, V. Gómez-Vallejo, M. Puigivila, A. Martín, T. Calvo-Fernández, S. E. Moya, R. F. Ziolo, T. Reese and J. Llop, Biodistribution of Different Sized Nanoparticles Assessed by Positron Emission Tomography: A General Strategy for Direct Activation of Metal Oxide Particles, *ACS Nano*, 2013, **7**(4), 3498–3505.

30 D. Liu, Q. Xia, D. Ding and W. Tan, Radiolabeling of Functional Oligonucleotides for Molecular Imaging, *Front. Bioeng. Biotechnol.*, 2022, **10**, DOI: **10.3389/fbioe.2022.986412**.

31 P.-O. Gendron, F. Avaltroni and K. J. Wilkinson, Diffusion Coefficients of Several Rhodamine Derivatives as Determined by Pulsed Field Gradient–Nuclear Magnetic Resonance and Fluorescence Correlation Spectroscopy, *J. Fluoresc.*, 2008, **18**(6), 1093–1101.

32 Jan Wolfgang Krieger and Jörg Langowski. QuickFit 3.0 (Status: Beta, Compiled: SVN:): A Data Evaluation Application for Biophysics. [web page] \verb + **http//www.dkfz.de/Macromol/quickfit/2015**.

33 P. Andreozzi, C. Simó, P. Moretti, J. M. Porcel, T. U. Lüdtke, M. Ramirez, A. de los, L. Tamberi, M. Marradi, H. Amenitsch, J. Llop, *et al.* Novel Core–Shell Polyamine Phosphate Nanoparticles Self–Assembled from PEGylated Poly (Allylamine Hydrochloride) with Low Toxicity and Increased In Vivo Circulation Time, *Small*, 2021, **17**(35), 2102211.

34 Z. B. Li, K. Chen, Z. Wu, H. Wang, G. Niu and X. Chen, 64Cu-labeled PEGylated polyethylenimine for cell trafficking and tumor imaging, *Mol. Imaging Biol.*, 2009, **11**(6), 415–423.

35 W. Yang, T. Miyazaki, Y. Nakagawa, E. Boonstra, K. Masuda, Y. Nakashima, P. Chen, L. Mixich, K. Barthelmes, A. Matsuoto, P. Mi and H. Cabral, Block catiomers with flanking hyrolyzable tyrosinate groups enhance in vivo mRNA delivery via *via* π-π stacking-assisted micellar assembly, *Sci. Technol. Adv. Mater.*, 2023, **24**(1), 2170164.

36 J. E. Zuckerman, C. H. J. Choi, H. Han and M. E. Davis, Polycation-siRNA nanoparticles can disassemble at the kidney glomerular basement membrane, *Proc. Natl. Acad. Sci. U. S. A.*, 2012, **109**(8), 3137–3142.